Phys. Lett. B 871 (2025) 140013

Contents lists available at ScienceDirect

Physics Letters B

journal homepage: www.elsevier.com/locate/physletb

Letter

Electromagnetic moments of ^{215,217}Bi: Probing shell evolution beyond $N = 126$

A. N. Andreyev [a], A. Barzakh [b,*], M. D. Seliverstov [b], Z. Yue [a], Menglan Liu [c], Cenxi Yuan [c], A. Algora [d,e], B. Andel [f], S. Antalic [f], M. Al Monthery [g], D. Atanasov [h,i], J. Benito [j], G. Benzoni [k], T. Berry [l], M. L. Bissell [m], K. Blaum [h], M. J. G. Borge [n], K. Chrysalidis [i,o], C. Clisu [p], T. E. Cocolios [q], C. Costache [p], J. G. Cubiss [r,a], T. Day Goodacre [s,i,m], G. J. Farooq-Smith [t,q], D. V. Fedorov [b], V. N. Fedosseev [i], L. M. Fraile [j], H. O. U. Fynbo [u], V. Gadelshin [o], L. P. Gaffney [v,w], R. F Garcia Ruiz [x,m], C. Granados [i,q], P. T. Greenlees [y], R. D. Harding [a,i], L. J. Harkness-Brennan [v], R. Heinke [i,o,m], A. Herlert [z], M. Huyse [q], A. Illana [aa], J. Jolie [ab], D. S. Judson [v], J. Karls [i,ac], J. Konki [y], P. Larmonier [i], I. Lazarus [ad], D. Leimbach [i,ac], R. Lică [p], Z. Liu [ae,af], D. Lunney [ag], K. M. Lynch [i,m], M. Madurga [ah], V. Manea [i], N. Marginean [p], R. Marginean [p], B. A. Marsh [i], C. Mihai [p], P. Molkanov [b], P. Mosat [f], M. Mougeot [i], J. R. Murias [j], E. Nacher [d], A. Negret [p], D. Neidherr [ai], L. Nies [i], R. D. Page [v], S. Pascu [p], A. Perea [n], V. Pucknell [ad], P. Rahkila [y], C. Raison [a], E. Rapisarda [i], K. Rezynkina [q], M. Rosenbush [aj,ak], R. E. Rossel [i], S. Rothe [i], V. Sánchez-Tembleque [j], K. Schomacker [ab], L. Schweikhard [aj], C. Seiffert [i], S. Sels [i,q], C. Sotty [p], L. Stan [p], M. Stryjczyk [q,al], D. Studer [o], J. Sundberg [i,ac], C. Sürder [am], O. Tengblad [n], P. Van Duppen [q], V. Vedia [j], M. Verlinde [q], S. Viñals [n], N. Warr [ab], A. Welker [i,an], F. Wienholtz [i,aj,am], R. N. Wolf [h,aj,ao]

[a] School of Physics, Engineering and Technology, University of York, YO10 5DD, York, United Kingdom
[b] Affiliated with an institute covered by a cooperation agreement with CERN at the time of the experiment, Russia
[c] Sino-French Institute of Nuclear Engineering and Technology, Sun Yat-Sen University, 519082, Zhuhai Guangdong, China
[d] Instituto de Física Corpuscular, CSIC - Universidad de Valencia, E-46980, Valencia, Spain
[e] HUN-REN Institute of Nuclear research (ATOMKI), P.O.Box 51, H-4001, Debrecen, Hungary
[f] Department of Nuclear Physics and Biophysics, Comenius University in Bratislava, 84248, Bratislava, Slovakia
[g] Physics Unit, College of Applied Sciences, University of Technology and Applied Sciences, P.O. Box 74, AL Khuwair, Muscat 133, Oman
[h] Max-Planck-Institut für Kernphysik, Saupfercheckweg 1, 69117, Heidelberg, Germany
[i] CERN, 1211, Geneva 23, Switzerland
[j] Grupo de Física Nuclear, Facultad de Ciencias Físicas, EMFTEL & IPARCOS, Universidad Complutense de Madrid, 28040, Madrid, Spain
[k] Istituto Nazionale di Fisica Nucleare, Sezione di Milano, I-20133, Milano, Italy
[l] Department of Physics, University of Surrey, GU2 7XH, Guildford, United Kingdom
[m] Department of Physics and Astronomy, The University of Manchester, M13 9PL, Manchester, United Kingdom
[n] Instituto de Estructura de la Materia, CSIC, Serrano 113 bis, E-28006, Madrid, Spain
[o] Institut für Physik, Johannes Gutenberg-Universität, D-55128, Mainz Mainz, Germany
[p] "Horia Hulubei" National Institute for R & D in Physics and Nuclear Engineering, RO-077125, Bucharest, Romania
[q] Instituut voor Kern- en Stralingsfysica, KU Leuven, B-3001, Leuven, Belgium
[r] School of Physics and Astronomy, University of Edinburgh, EH9 3FD, Edinburgh, United Kingdom
[s] TRIUMF, 4004 Wesbrook Mall, V6T 2A3, Vancouver, BC, Canada
[t] Department of Oncology Physics, Edinburgh Cancer Centre, Western General Hospital, Crewe Road South, EH4 2XU, Edinburgh, United Kingdom
[u] Department of Physics and Astronomy, Aarhus University, DK-8000, Aarhus C, Denmark
[v] Oliver Lodge Laboratory, University of Liverpool, L69 7ZE, Liverpool, United Kingdom
[w] School of Engineering and Computing, University of the West of Scotland, PA1 2BE, Paisley, United Kingdom
[x] Department of Physics, Massachusetts Institute of Technology, Cambridge, USA
[y] Department of Physics, University of Jyväskylä, P.O. Box 35, FI-40014, Jyväskylä, Finland

* Corresponding author.
E-mail address: barzakh_ae@pnpi.nrcki.ru (A. Barzakh).

https://doi.org/10.1016/j.physletb.2025.140013
Received 29 May 2025; Received in revised form 16 September 2025; Accepted 4 November 2025
Available online 7 November 2025

[z] FAIR GmbH, Planckstraße 1, 64291, Darmstadt, Germany
[aa] Istituto Nazionale di Fisica Nucleare, Laboratori Nazionali di Legnaro, I-35020, Legnaro, Italy
[ab] Institut für Kernphysik, Universität zu Köln, 50937, Köln, Germany
[ac] Department of Physics, University of Gothenburg, SE-412 96, Gothenburg, Sweden
[ad] STFC Daresbury, WA4 4AD, Daresbury Warrington, United Kingdom
[ae] Institute of Modern Physics, Chinese Academy of Sciences, 730000, Lanzhou, China
[af] School of Nuclear Science and Technology, University of Chinese Academy of Sciences, 100049, Beijing, China
[ag] CSNSM-CNRS, Université de Paris Sud, 91400, Orsay, France
[ah] Department of Physics and Astronomy, University of Tennessee, 37996, Knoxville, Tennessee, USA
[ai] GSI Helmholtzzentrum für Schwerionenforschung GmbH, 64291, Darmstadt, Germany
[aj] Institut für Physik, Universität Greifswald, 17487, Greifswald, Germany
[ak] Center for Accelerator-Based Science, RIKEN Nishina, 351-0198, Wako, Saitama, Japan
[al] Institut Laue-Langevin, 71 Avenue des Martyrs, F-38042, Grenoble, France
[am] Institut für Kernphysik, Technische Universität Darmstadt, 64289, Darmstadt, Germany
[an] Institut für Kern- und Teilchenphysik, Technische Universität Dresden, 01069, Dresden, Germany
[ao] School of Physics, ARC Centre of Excellence for Engineered Quantum Systems, The University of Sydney, 2006, NSW, Australia

ARTICLE INFO

Editor: Prof. Betram Blank

Keywords:
Laser spectroscopy
Hyperfine structure
Dipole magnetic moments
Shell-model calculations

ABSTRACT

The nuclear properties of bismuth isotopes ($Z = 83$), with just one valence proton above the closed spherical shell at $Z = 82$, are expected to be governed by a single unpaired proton. However, already in semimagic ^{209}Bi ($Z = 83$, $N = 126$), the magnetic moment (μ) strongly deviates from the single-particle Schmidt value. A near linear decrease in μ with the increase of N after the $N = 126$ magic number was observed up to $N = 130$. In order to test whether this trend is kept at $N > 130$ and to reveal the underlying mechanisms, an investigation of ^{215,217}Bi ($N = 132, 134$) has been undertaken. The magnetic dipole and electric quadrupole moments of the $I^{\pi} = 9/2^{-}$ nuclear ground states in these isotopes have been measured for the first time using the in-source resonance-ionization spectroscopy technique at ISOLDE (CERN). It has been shown that the linearly decreasing trend of $\mu(^{209,211,213}\mathrm{Bi}^{g})$ is broken in ^{215,217}Bi with a nearly constant value of μ observed. Experimental data have been compared to calculations in the framework of the configuration-interaction shell model with the monopole-based universal $\mathrm{V_{MU}}$ + LS interaction. The peculiarities in the behavior of μ(Bi, $9/2^{-}$) with increasing neutron number are explained as being due to the shell evolution, change of the neutron orbitals occupancies and strong configuration mixing beyond $N = 130$. Also, the difference in the μ trends for bismuth ($Z = 83$) and astatine ($Z = 85$) isotopes with $N > 126$ are reproduced by the shell-model calculations. It is shown that monopole interaction plays noticeable role in the description of the peculiarities of the μ behaviour. Additionally, the extension of the application of the $\mathrm{V_{MU}}$ interaction to the μ isotopic trends for heavy nuclei is important for further study of the capabilities of this promising version of the shell-model calculations.

1. Introduction

One of the key properties of atomic nuclei are the values of their magnetic dipole and electric quadrupole moments. The spectroscopic electric quadrupole moment (Q_s) probes the collective degrees of freedom (e. g., deformation), whereas the magnetic dipole moment (μ) is closely connected with the single-particle properties of the nucleus. Their description as a function of neutron number within the isotopic chains, especially the irregularities which are often observed near shell closures, provide a crucial benchmark for nuclear theory (see, e.g., Refs. [1–5] and references therein).

For example, the magnetic moment of the $I^{\pi} = 5/2^{+}$ odd-A europium ($Z = 63$) ground states reaches a maximum at the neutron shell closure at $N = 82$ with a near-linear decrease on both sides of the closed neutron shell ($78 \leq N \leq 88$; see Fig. 4 in Ref. [6]). Similar kinks were also observed for the thallium ($Z = 81$) and indium ($Z = 49$) isotopic chains at the neutron magic numbers $N = 126$ and $N = 82$, respectively [3,7,8].

In this respect, the bismuth isotopic chain ($Z = 83$) is especially interesting since bismuth has just one $h_{9/2}$ proton above the shell closure at $Z = 82$. However, even for semimagic ^{209}Bi, one finds a very large deviation from the single-particle Schmidt value: $\mu_{\mathrm{Schmidt}}(^{209}\mathrm{Bi}) = 2.6\,\mu_N$, $\mu_{\mathrm{expt}}(^{209}\mathrm{Bi}) = 4.1\,\mu_N$ [9]. Furthermore, similar to the aforementioned cases, a near linear decrease in μ on both sides of the $N = 126$ magic number was observed, albeit with different gradients.

The isotopic μ trend for isotonic astatine isotopes was found to display the close resemblance to the μ trend for the bismuth nuclei with $N < 126$ [10]. It was expected that this similarity is preserved also at $N > 126$. Indeed, throughout the nuclide chart the isotopic dependencies of μ for nuclei with the same spin and parity are very similar, see, for example, systematics of $\mu(11/2^{-})$, $\mu(7/2^{+})$ values in odd-Z, even-N isotopes, see Refs. [3,5,11] and references therein. However, prior to the present work, magnetic moments for the bismuth $9/2^{-}$ ground states was known only up to $N = 130$ [12–14] whereas in the astatine isotopic chain, isotopes with $N = 128, 130$ have very short lifetimes (125 ns and 100 μs, respectively) and cannot be studied by laser spectroscopy. In order to provide an opportunity to compare $\mu(9/2^{-})$ trends for bismuth and astatine isotopes at $N > 126$ and to reveal the underlying mechanisms, in the present work μ of ^{215,217}Bi ($N = 132, 134$) has been measured.

On the theory side, impressive descriptions of μ in several long isotopic chains have been achieved by the deformed energy-density functional calculations with accounting for the time-odd terms [1,2,4,5,8] and in the framework of the theory of finite Fermi systems based on the Fayans functional [3,15–18]. However, both approaches fail to reproduce experimental μ for bismuth isotopes near $N = 126$.

As indicated in Ref. [4], this discrepancy is most likely due to specific configuration mixing. Such configuration mixing should be strongly dependent on the number of neutrons outside the closed shell and, correspondingly, might be a source of the observed behavior of μ.

Recently, significant progress was achieved in the large-scale shell model calculations in the region near ^{208}Pb (see Refs. [19–25] and references therein). In particular, the monopole-based universal interaction $\mathrm{V_{MU}}$ was introduced [26] in order to construct shell-model Hamiltonians for different model spaces in a unified way. For example, this interaction was used to understand the recently-discovered isomeric states in ^{213,215}Tl, where shell evolution plays a significant role [21,27]. In order to further test this interaction, a comparison of the corresponding shell-model calculations with the experimental data for μ and Q_s near $N = 126$ was implemented in the present work.

2. Experimental details

The experiments were performed at the ISOLDE facility (CERN) [28]. The bismuth nuclei were produced in spallation reactions induced by the 1.4-GeV proton beam from the CERN PS Booster impinging on a thick UC_x target (50 g cm^{-2} of ^{238}U). The spallation products effused out of the high-temperature target ($T \approx 2500$ K) as neutral atoms into the cavity of the Resonance Ionization Laser Ion Source, RILIS [29]. The bismuth atoms were resonantly ionized when the laser beams were wavelength-tuned to a three-step ionization scheme [30,31]. The hyperfine structure (hfs) measurements were performed for the first-step transition of the ionization scheme, $6p^3\ ^4S^o_{3/2} \rightarrow 6p^2(^3P_0)7s\ ^2[0]_{1/2}$ ($\lambda_1 = 306.9$ nm) by scanning the frequency of a narrowband Titanium Sapphire laser [32]. The produced photoions were extracted and accelerated by a 30-kV potential and mass separated by ISOLDE's General Purpose Separator.

Data were collected during three separate experimental runs which differ by the method of the photoion-current monitoring. During the first experimental campaign (2016) the photoion current of ^{215,217}Bi was monitored by ion counting with a Multi-Reflection Time-of-Flight Mass-Separator (MR-ToF MS, [33,34]). In the second and third runs (2017, 2018) the ISOLDE Decay Station (IDS) [35] was used for decay-based ion-current monitoring. Partial results from these experimental campaigns can be found in Refs. [24,25,36] ($^{187-191,214,216}$Bi).

3. Results

Over three experimental campaigns, seven hfs spectra were measured for ^{215}Bi^g and four for ^{217}Bi. Fig. 1 provides typical examples. Note, that intensities ratios of the ^{217}Bi hyperfine components on Fig. 1 do not correspond to the theoretical values due to saturation and not optimal fixation of the second-step transition frequency. These distortion factors were explicitly taken into account in the fitting procedure [10,31].

The positions of the hyperfine components in the hfs spectra are determined by the standard relation [37] with five parameters: nuclear spin (I), isotope shift relative to the stable ^{209}Bi ($\delta\nu_{A,209}$), magnetic hfs constants (a_1 and a_2) for the first ($6p^3\ ^4S^o_{3/2}$) and the second ($6p^2(^3P_0)7s\ ^2[0]_{1/2}$) level of the ionization scheme, and electric quadrupole hfs constant b_1 for the first atomic level. Note, that the quadrupole hfs constant for the second level $b_2 \equiv 0$ since the second level has total electronic angular momentum $J = 1/2$.

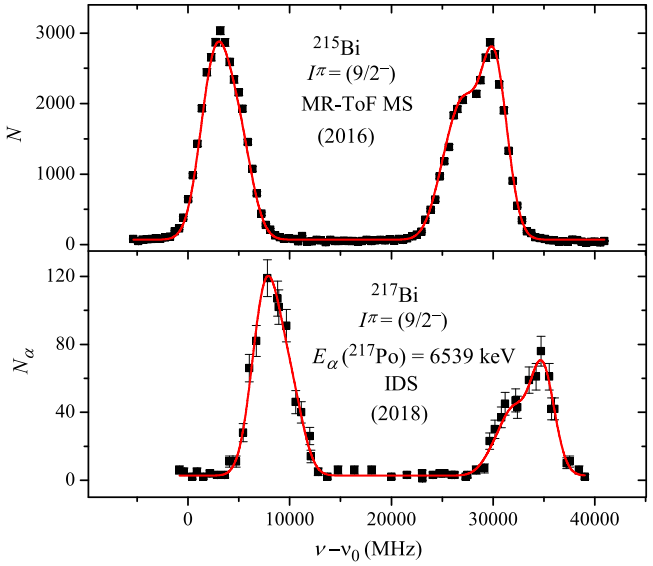

Fig. 1. Examples of the hfs spectra of ^{215,217}Bi^g. The nuclear spins, detection method and the year of experiment are shown. In the case of ^{217}Bi, the energy of the α particles from the decay of daughter ^{217}Po ($T_{1/2} = 1.53(5)$s) produced after ^{217}Bi β decay, is also indicated. They were used for monitoring the photoion rate. The solid lines depict the Voigt-profile fit to the data. The zero point on the frequency scale corresponds to a wave number of 32588.16 cm^{-1}.

Table 1
Hfs constants (a_2, b_1), magnetic (μ) and quadrupole (Q_s) moments for ^{215,217}Bi.

A	I^π	$T_{1/2}$(s)	a_2 (MHz)	$\mu(\mu_N)$[a]	b_1(MHz)	Q_s(b)
215	$(9/2^-)$	456(12)	4423(40)	3.675(33){18}	−397(150)	−0.55(21)
217	$(9/2^-)$	98.5(13)	4465(50)	3.710(42){19}	−520(150)	−0.72(21)

[a] The statistical and systematic uncertainties are shown in round and curly brackets, respectively. The latter values originate from the uncertainty of the hyperfine anomaly.

Due to the limited resolution of the RILIS method we cannot determine the nuclear spin from the hfs spectra. Therefore, we used available information on the spin values obtained by nuclear spectroscopy. For ^{215,217}Bi^g a spin of $I = 9/2$ was used, in accordance with systematics, beta decay pattern [38–40], the structure of excited states [41] and shell-model calculations [38,41].

The experimental data were fitted with Voigt profiles (more details are in Ref. [31]). In the fit, the ratio $\rho = a_2/a_1$ was fixed according to its value for ^{209}Bi: $\rho(^{209}\text{Bi}) = -11.013(4)$ [9,42]. The fitting results from the different runs agree with each other within the limits of uncertainties and the final values of the hfs constants shown in Table 1, are the corresponding weighted means.

From the hfs constants, the nuclear μ and Q_s values were deduced, relative to those of ^{209}Bi taken from Refs. [9,36]. High-resolution hfs measurements for lighter bismuth isotopes demonstrate that the hyperfine anomaly (HFA) for bismuth isotopes with spin 9/2 is less than 0.5% [43]. Corresponding uncertainties were taken into account for deduced μ values. The values of μ and Q_s are presented in Table 1.

3.1. Magnetic moments

In Fig. 2, the g factors ($g = \mu/I$) for the $\pi h_{9/2}$ ground states in $_{83}$Bi, $_{85}$At and $_{87}$Fr isotopes near $N = 126$ are shown. The spin and parity assignment $I^\pi = (9/2^-)$ for the ^{217,219}At ground states is based on the low hindrance factors, $HF = 1.1$ and 1.16(4), of their α decays to the ground states of ^{213,215}Bi, which have established $I^\pi = (9/2^-)$ assignment [44,45]. The spin and parity assignment for the ^{219,221}Fr ground states ($I^\pi = 9/2^-$ and $5/2^-$) are reliably established as well, and both states have leading $\pi h_{9/2}$ configuration, despite the change in spin from 9/2 to 5/2, see Refs. [46,47].

Note, that in the astatine and francium isotopic chains, some key isotopes ($N = 128, 130$) have very short lifetimes and cannot be studied with laser-spectroscopy measurements. Thus, the bismuth isotopes represent a unique chain where information on $\mu(h_{9/2})$ at $128 \le N \le 134$ can be obtained without gaps.

The isotopic dependence of g(Bi, $9/2^-$) strikingly deviates from that for the adjacent astatine and francium isotopic chains at $N > 130$. Instead of a rapid decrease with increasing N, as seen in astatine and francium isotopes, one can see the stabilization of g(Bi, $9/2^-$) whereby $g(^{213}\text{Bi}^g)$ coincides with $g(^{215,217}\text{Bi}^g)$ within the limits of uncertainties.

The $9/2^-$ ground states in ^{215,217}Bi and ^{217,219}At are considered to be predominantly spherical $h_{9/2}$ states, see Refs. [41,51] and references therein. In contrast, neutron-rich francium isotopes are known to have a moderate quadrupole deformation and exhibit parity doublet bands and inverse odd-even staggering in radii, associated with octupole deformations [52–54]. Moreover, ground states of ^{219,221}Fr are supposed to be the band heads of strongly Coriolis-perturbed rotational bands built on the $\pi 1/2^-[541]h_{9/2}$ Nilsson orbital.

An obvious difference in the interpretation of the $9/2^-$ ground states in the isotonic francium, and astatine and bismuth nuclei, explains the sharp decrease of $g(^{219,221}\text{Fr})$ in comparison with $g(^{215,217}\text{Bi})$ and

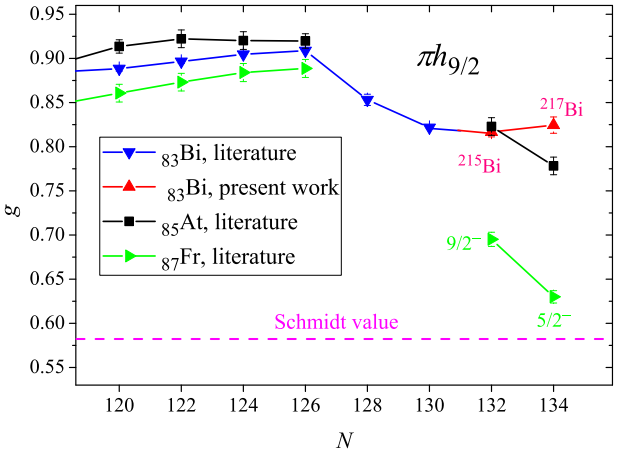

Fig. 2. g factors for the $\pi h_{9/2}$ ground states in $_{83}$Bi (red upward triangles: present work; blue downward triangles: Refs. [12,13]), $_{85}$At (black squares: Refs. [10, 48]) and $_{87}$Fr (green rightward triangles: Refs. [49,50]) isotopes. The data points without labels correspond to the nuclei with $I^{\pi} = (9/2^{-})$. The data points are connected by lines to guide the eyes.

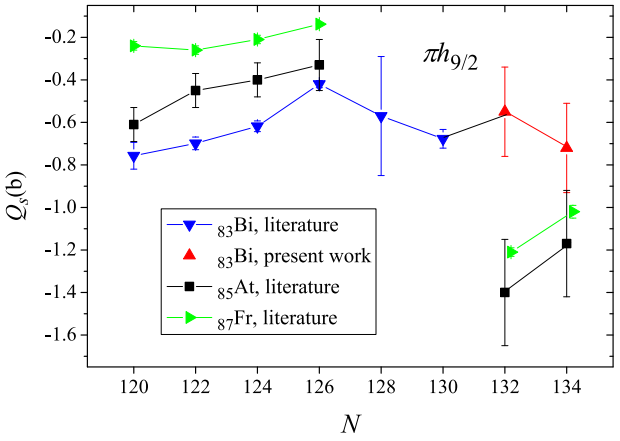

Fig. 3. Spectroscopic quadrupole moments for $\pi h_{9/2}$ ground states in $_{83}$Bi (red upward triangles: present work; blue downward triangles: Refs. [12,13]), $_{85}$At (black squares: Ref. [10,48]) and $_{87}$Fr (green rightward triangles: Refs. [49,50]) isotopes. The data points are connected by lines to guide the eyes.

$g(^{217,219}\mathrm{At})$, see Fig. 2. Namely, calculations in the framework of the Nilsson model with effective decoupling parameter describe magnetic moments of the $5/2^{-}$ and $9/2^{-}$ band members of the $\pi 1/2^{-}[541]h_{9/2}$ band fairly well [34].

Below (Section 4) we will not consider deformed francium isotopes in our shell-model calculations which are restricted to spherical nuclei. The assumption of spherical symmetry for ^{215,217}Bi and ^{217,219}At [41,51] will be additionally justified by the good agreement of the spherical theory and experiment for the magnetic moments of these nuclei (Section 4).

3.2. Quadrupole moments

In Fig. 3, the quadrupole moments for $\pi h_{9/2}$ ground states in $_{83}$Bi, $_{85}$At and $_{87}$Fr are shown. The isotopic dependence of Q_s(Bi, $9/2^{-}$) differs from the common pattern for the adjacent astatine and francium isotopic chains. However, this deviation cannot be regarded as well established due to the large uncertainties.

As was stressed in [48], surprisingly, despite an obvious difference in the interpretation of the $9/2^{-}$ ground states in the isotonic francium and astatine nuclei, the corresponding quadrupole moments have nearly the same values. Before drawing any conclusions, it would be highly desirable to remeasure Q_s(Bi, $9/2^{-}$) and Q_s(At, $9/2^{-}$) with reduced uncertainty.

In view of the difference of the μ (and, possibly, Q_s) behaviour for bismuth and astatine isotopes, it is important to compare the $\delta\langle r^2\rangle$ values for these nuclei. As seen in Fig. 4, isotopic $\delta\langle r^2\rangle$ dependencies for bismuth and astatine are very similar and there are no irregularities at $N = 132$ or 134.

4. Shell-model calculations

The μ and Q_s values of odd-A bismuth and astatine isotopes in the vicinity of $N = 126$ shell closure were calculated in the framework of the configuration-interaction shell model (CISM) [19], using the expression (Refs. [20,56]):

$$\mu = g_L^{\mathrm{eff}}(p)L_p + g_L^{\mathrm{eff}}(n)L_n + g_s^{\mathrm{eff}}(p)s_p + g_s^{\mathrm{eff}}(n)s_n \qquad (1)$$

where $L_{p,n}$ and $s_{p,n}$ are the proton and neutron angular momentum and spin terms of the nuclear matrix elements, respectively.

In Eq. (1), the effective orbital and spin g factors for protons and neutrons ($g_L^{\mathrm{eff}}(p,n)$ and $g_s^{\mathrm{eff}}(p,n)$) were used instead of the free ones since the shell-model calculations were performed in the truncated model space. A renormalization of the $g_L(p)$ factor was also applied, which

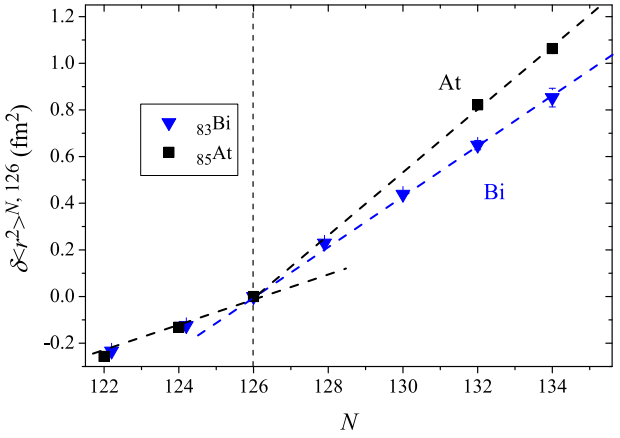

Fig. 4. Changes in the mean-squared charge radii for bismuth (downward triangles, [12,13,55]) and astatine (squares, [10,48]) odd-A isotopes near $N = 126$.

was recently determined by the measurement of $\mu(^{207}\mathrm{Tl}^{m}, \pi h_{11/2})$ [3], $g_L^{\mathrm{eff}}(p) = 1.095(11)$.

There are several estimations of $g_L^{\mathrm{eff}}(n)$ in the lead region. Nearly all of them fall within the interval [-0.03, -0.05], see Refs. [57,58] and references therein. In our shell-model calculations a mean value of $g_L^{\mathrm{eff}}(n) = -0.04$ was used.

The choice of the g_s-factor renormalization (the same for protons and neutrons) was based on the condition of the best agreement with the experimental data for the ground-state magnetic moment of the odd-A bismuth isotopes with $A = 203 - 217$. The result, $g_s^{\mathrm{eff}} = 0.57 g_s^{\mathrm{free}}$, where g_s^{free} is the g_s factor of the free nucleon, is reasonably consistent with the commonly used g_s-factor renormalization (see, for example, Ref. [20]).

The departure of μ from the Schmidt value is often considered in terms of the first-order (CP1) and second-order (CP2) core-polarization corrections, as well as the meson-exchange current contribution (see Ref. [59] and references therein). The latter can be accounted for by the orbital g factor renormalization. CP2 comes from the valence-nucleon coupling with the low-lying collective excited states of the core ($2^{+}, 3^{-}$, etc.). This type of mixing cannot be taken into account in the framework of the CISM calculations. Nevertheless, an important correction of the second order could be connected with a tensor component of the $M1$ operator. Previous studies in the framework of CISM [20] indicated that the second-order $M1$ operator has very limited influence on the magnetic moment. Therefore, in our case, we did not include this term. The contribution from the CP1 correction was effectively accounted for

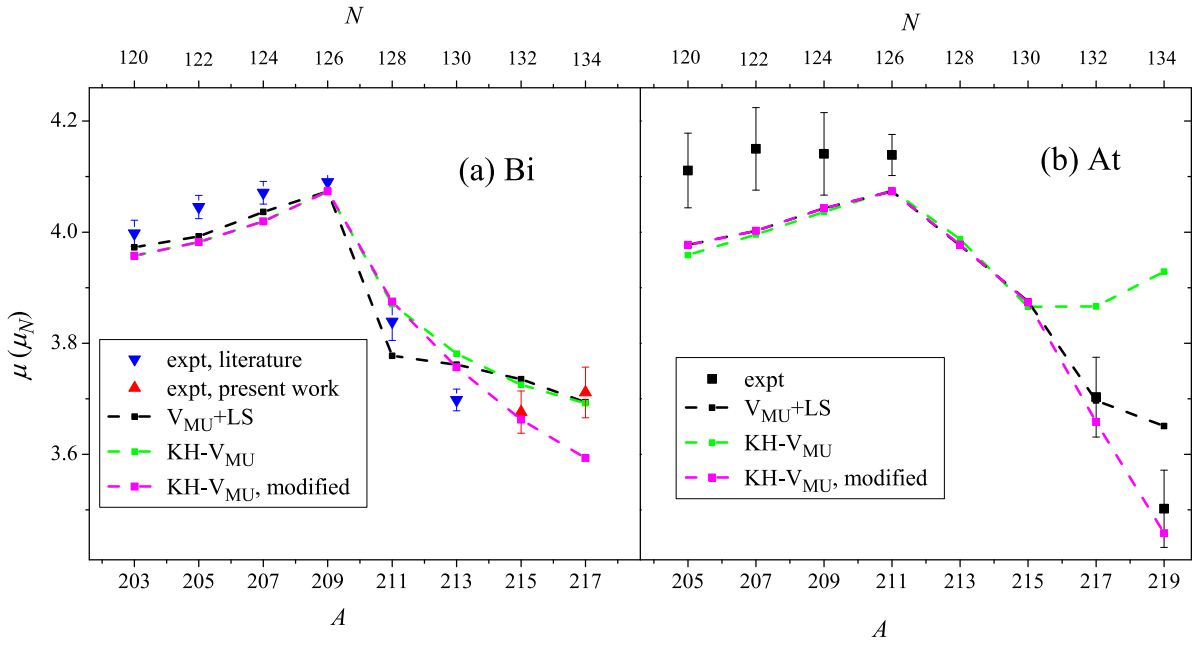

Fig. 5. Comparison of μ values from experiment and CISM calculations for $I^{\pi} = 9/2^{-}$ states of bismuth and astatine isotopes. (a) Bismuth isotopes. Upward triangles: experiment, present work; downward triangles: experiment, Refs. [12,13]). (b) Astatine isotopes. Squares: experiment, Refs. [10,48]. Black and green lines correspond to the V_{MU} + LS and KH-V_{MU} interaction, respectively. Magenta lines correspond to the KH-V_{MU} interaction with modified monopole matrix element (see text for details).

by the renormalization of the g_s factor. The renormalization of the g_s and g_L factors has not noticeable effect on the μ trends. It shifts the theoretical curve as a whole.

Quadrupole moments were calculated by the formula:

$$Q_s = e_p Q_p + e_n Q_n, \tag{2}$$

where $Q_{p,n}$ are the proton and neutron quadrupole matrix elements and e_p (e_n) denotes proton (neutron) effective charge induced by in-medium and core-polarization effects. We accepted the standard values $e_p = 1.5$ and $e_n = 0.5$ [60,61] and did not apply the optimization procedure for these effective charges owing to the large uncertainties in the experimental Q_s values, see Table 1 and Fig. 3.

The shell-model calculations were performed using the code KSHELL [62] in two model spaces: $jj66$ ($82 < Z, N < 126$) (neutron-deficient isotopes) and $jj67$ ($82 < Z < 126, 126 < N < 184$) (neutron-rich isotopes) [19]. Neutron excitations across the $N = 126$ shell gap were not taken into account. The same set of strength parameters was used for both model spaces, $jj66$ and $jj67$. For ^{217,219}At and ^{217}Bi a monopole-based truncation was implemented with a threshold of 5 MeV. This method was applied and described in detail in Ref. [63].

Two effective interactions were used. The first one was constructed from the monopole-based universal interaction V_{MU} (Refs. [26,64]) and the M3Y type of spin-orbit interaction [65] (V_{MU} + LS). The V_{MU} interaction contains a Gaussian central force and a bare $\pi + \rho$ meson exchange tensor force. The strengths of the central forces were changed in accordance with Refs. [26,64]. Namely, the proton-proton (neutron-neutron) central forces were enhanced by 15% (5%) to enable a more accurate description of the low-lying excitation energies in medium-heavy nuclei [19,63,66].

The interaction parameters were the same as used in Ref. [63] for the ^{132}Sn region. CISM calculations with the V_{MU} + LS interaction were successfully performed in different regions of the nuclide chart (see Refs. [19–21,66] and references therein). Note, that earlier one had to choose different effective Hamiltonians with different origins for different nuclear regions. It is of great significance that the V_{MU} + LS interaction enables one to construct effective Hamiltonians for several regions from one basis. More detailed information about the V_{MU} + LS interaction can be found in Ref. [19].

The second effective interaction combines the Kuo-Herling and V_{MU} interactions. For the $jj66$ model space, the $p - p$, $n - n$, and $p - n$ parts of two-body interactions were taken from the Kuo-Herling particle interaction (KHPE) [67], Kuo-Herling hole interaction (KHHE) [68], and V_{MU} interaction [26], respectively (see application of the same combined interaction for the $jj66$ model space in Ref. [69]). Another combination of Kuo-Herling and V_{MU} + LS interactions was proposed in Ref. [20].

Note that the KHHE interaction was constructed in the $jj56$ model space ($50 < Z < 82$ and $82 < N < 126$). There is no Kuo-Herling interaction for the proton-neutron part in the $jj66$ model space. Correspondingly, we were forced to use the "combined" interaction with the V_{MU} effective nuclear force in the $p - n$ sector, to address this issue.

The results of the calculations are compared with the experimental data in Fig. 5. As one can see, all trends in μ(Bi, $9/2^{-}$) isotopic behavior are reproduced by both interactions: namely the decrease of μ on the both sides of $N = 126$, the more rapid drop for $N > 126$ than $N < 126$, and the flattening at $N = 130, 132, 134$. However, the V_{MU} + LS interaction better models the abrupt transition from the steep decrease to near constancy of μ in accordance with experimental data compared to the KH-V_{MU} interaction which displays a smoother transition. Remarkably, the V_{MU} + LS interaction also describes μ(At, $9/2^{-}$) isotopic behavior fairly well, reproducing the unexpected difference between bismuth and astatine isotopic chains. At the same time, the KH-V_{MU} interaction fails in describing the regular monotonic decrease of μ(At, $9/2^{-}$) with the increase of N for $N > 130$.

Both shell-model calculations give similar results for the Q_s values and reproduce the trend of the quadrupole moments for bismuth isotopes near $N = 126$ (see Fig. 6). However, a more detailed analysis is not possible due to the large experimental uncertainties.

5. Discussion

In the framework of the CISM calculations, the isotopic trend of the magnetic moments is determined by the subtle interplay between interlinked mechanisms. These are the evolution of the effective single-

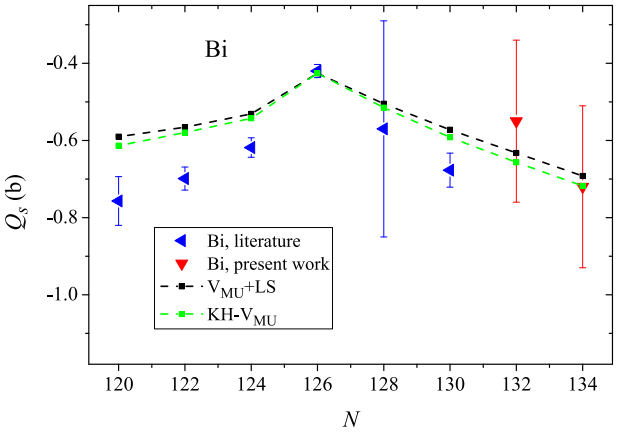

Fig. 6. Comparison of the CISM calculations of quadrupole moments for $9/2^-$ ($\pi h_{9/2}$) bismuth ground states with experimental data. Downward triangles: present work; leftward triangles: Refs. [12,13]; dot-dashed and dashed lines correspond to the V_{MU}+LS and KH-V_{MU} interaction, respectively. Theoretical points are connected by lines to guide the eyes.

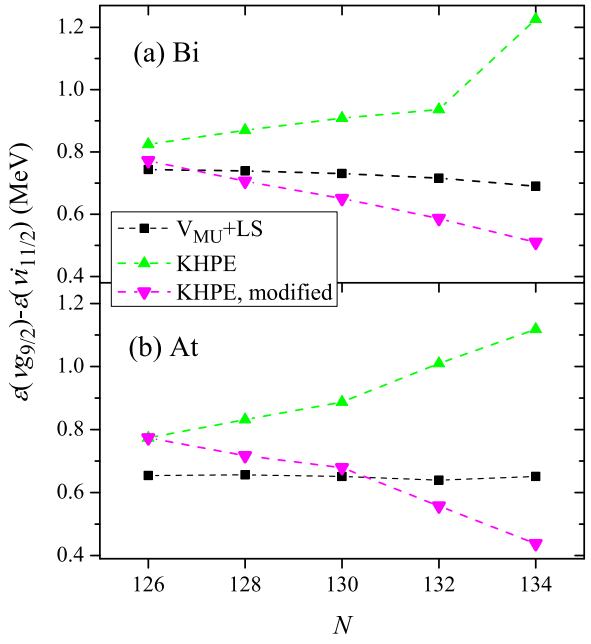

Fig. 7. The gap between $\nu 0i_{11/2}$ and $\nu 1g_{9/2}$ orbitals for (a) bismuth and (b) astatine isotopes at $N > 126$. Squares and triangles correspond to V_{MU}-LS and KHPE interactions, respectively. Open symbols show the results of calculation with modified monopole matrix element (see text for details).

particle energies (ESPE) due to the monopole interaction [26,64], the change in occupancies of the shell-model states, and configuration mixing. The evolution of the ESPE, in particular, changes the energy difference between $\nu 0i_{11/2}$ and $\nu 1g_{9/2}$ orbitals (see Fig. 7).

In Fig. 8, the percentage of the main neutron components in the wavefunction of the bismuth ground states is shown for the V_{MU}+LS interaction. Naively, one would expect a dominant $\pi 1h_{9/2} \otimes \nu 1g_{9/2}^{N-126}$ configuration when neutrons successively fill the $\nu 1g_{9/2}$ orbital, which is closest to the Fermi level (see inset in Fig. 8). However, one observes that the occupancy of this configuration rapidly drops with increasing N, and after $N = 130$ the leading configuration becomes $\pi 1h_{9/2} \otimes (\nu 1g_{9/2}^{N-128} \otimes \nu 0i_{11/2}^2)$. Moreover, for $N > 126$ the configuration component with two neutrons in the $\nu 0j_{15/2}$ orbital also becomes larger than that with only the $\nu 1g_{9/2}$ neutron orbital occupied. As the magnetic moment strongly depends on the configuration, the different mixing leads to a different trends in μ values for bismuth and astatine isotopes with $N > 130$ (Fig. 5). A similar picture with a dramatic change in the underlying configurations is also seen in the calculations using the KHPE interaction.

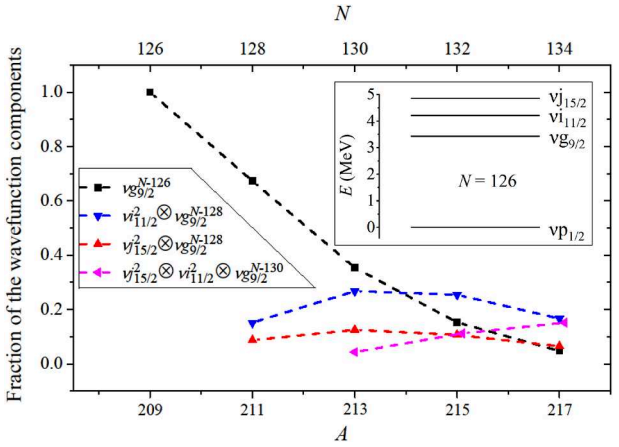

Fig. 8. Fraction of the wavefunction components for Bi isotopes with $N \geqslant 126$ (V_{MU} + LS interaction). In the inset, schematic diagram of the neutron single-particle orbitals above $N = 126$ is shown.

It should be noted that the reduction of the energy gap between the $\nu 0i_{11/2}$ and $\nu 1g_{9/2}$ orbitals when using the V_{MU} + LS interaction (see Fig. 7) not only favors the excitation of a single neutron from $\nu 1g_{9/2}$ to $\nu 0i_{11/2}$, but makes much more probable the scattering of pairs of neutrons from the lower to the higher orbitals due to pairing.

Let us now consider the difference between the $\mu(9/2^-)$ trends for bismuth and astatine isotopes with $N > 126$. The occupancy of the $\nu 0j_{15/2}$ orbital lowered the ESPE of the $\nu 0i_{11/2}$ orbital, which becomes closer to that of the $\nu 1g_{9/2}$ orbital. This increases the occupancy of the $\nu 0i_{11/2}$ orbital, decreasing the value of $\mu(9/2^-)$. At the same time, neutrons occupying the $\nu 0i_{11/2}$ orbital push it away from $\nu 1g_{9/2}$. The competition between the two mechanisms results in the observed decrease and then stabilization of $\mu(9/2^-)$ in bismuth isotopes with $N > 126$.

In contrast with bismuth nuclei, in astatine isotopes there are extra protons which occupy the $\pi 1h_{9/2}$, $\pi 1f_{7/2}$ and $\pi 0i_{13/2}$ orbitals. Adding protons to the $\pi 0i_{13/2}$ orbital pulls the $\nu 1g_{9/2}$ and $\nu 0i_{11/2}$ orbitals closer due to the neutron-proton tensor interaction. Therefore, the balance achieved in bismuth isotopes at $N = 132, 134$ is broken in the isotonic astatine nuclei, resulting in the different trends for $\mu(9/2^-)$ in these chains (see Fig. 2).

The difference in the μ(At, $9/2^-$) description by the KH-V_{MU} and V_{MU} + LS interactions can also be explained by the difference in the corresponding shell-evolution pictures. The KH-V_{MU} interaction overestimates the gap between $\nu 1g_{9/2}$ and $\nu 0i_{11/2}$ shells. Moreover, this gap increases when adding neutrons to the valence space in the KHPE calculations, while it decreases in the V_{MU} + LS case (see Fig. 7). As a result, the calculated KH-V_{MU} magnetic moment of ^{217,219}At increases and deviates from the experimental value [see Fig. 5(b)].

In order to check the influence of the monopole part of the interaction, the monopole matrix elements $\langle \nu 1g_{9/2}, \nu 1g_{9/2}|V|\nu 1g_{9/2}, \nu 1g_{9/2}\rangle$ of KHPE were artificially increased by 0.1 MeV. As a result, the ESPE of the $\nu 1g_{9/2}$ orbital increased for all nuclei considered, and the dominant configuration of the ground state of ^{219}At proved to be $(\pi 1h_{9/2})^3 \otimes (\nu 1g_{9/2})^6 \otimes (\nu 0i_{11/2})^2$ rather than $(\pi 1h_{9/2})^3 \otimes (\nu 1g_{9/2})^8$. Correspondingly, KHPE magnetic moments of astatine isotopes becomes closer to the experimental data [see Fig. 5(b)].

6. Summary

To summarize, the hfs of the 306.9-nm atomic transition was studied for ^{215,217}Bi^g using the in-source resonance-ionization spectroscopy tech-

nique. Magnetic dipole and electric quadrupole moments were derived from the experimental data. The isotopic dependency of μ(Bi, $9/2^-$) deviates strikingly from the pattern in the adjacent astatine isotopic chain.

Magnetic moments [μ(Bi, $9/2^-$) and μ(At, $9/2^-$)] were calculated within the framework of the CISM with KH-V_{MU} and V_{MU} + LS interactions. The peculiarities in the μ(Bi, At, $9/2^-$) isotopic behavior (in particular, the different patterns for bismuth and astatine at $N > 126$) are well reproduced by the calculations with V_{MU} + LS interactions. However, the KH-V_{MU} interaction fails to describe the μ(At, $9/2^-$) values for $N > 126$. The difference between the μ(At, $9/2^-$) and the μ(Bi, $9/2^-$) isotopic dependencies, as well as the difference between calculation results with different interactions are related to the configuration mixing and shell-evolution effects. Quadrupole moments of bismuth-isotopes ground states near $N = 126$ are described by CISM calculations with both interactions fairly well.

Notably, magnetic moments of astatine isotopes with $N = 132, 134$ were described without the appeal to octupole deformation although there are some evidence in favor of the reflection asymmetry for these nuclei [48,55].

Our inference on the increased occupation of the high-j $\nu 0i_{11/2}$ and $\nu 0j_{15/2}$ neutron orbitals above $N = 126$ may be further relevant to the discussion of their role in producing the kink in the mean-square charge radii in the lead, mercury and thallium isotopic chains [70–73].

Data availability

No data was used for the research described in the article.

Declaration of competing interest

The authors declare the following financial interests/personal relationships which may be considered as potential competing interests: Menglan Liu, Cenxi Yuan, Z. Liu reports financial support was provided by National Natural Science Foundation of China. R. Lica, N. Marginean, R. Marginean, C. Costache, C. Clisu reports financial support was provided by Romanian IFA. J. Benito, L. M. Fraile, J. R. Murias, V. Vedia reports financial support was provided by Complutense University of Madrid. A. Algora, E. Nacher reports financial support was provided by Generalitat Valenciana PROMETEO CIPROM. B. Andel, S. Antalic reports financial support was provided by Slovak Research and Development Agency. If there are other authors, they declare that they have no known competing financial interests or personal relationships that could have appeared to influence the work reported in this paper.

Acknowledgments

We thank the ISOLDE Collaboration for providing excellent beams. Shell model calculations have been supported by the National Natural Science Foundation of China under Grant No. 12475129. A. A. is grateful for financial support from the Chinese Academy of Sciences President's International Fellowship Initiative (Grant No. 2020VMA0017). Z. L. was supported by the National Natural Science Foundation of China (Grant No. 12135004). This work was supported by Spanish MCIN/AEI/10.13039/501100011033 under grant No. RTI2018-098868-B-I00 and No. PID2021-126998OB-I00. J.G.L. acknowledges financial support by the National Natural Science Foundation of China under Grant No. 11874090. This work was supported by the Romanian IFA grant CERN/ISOLDE and Nucleu project No. PN 23 21 01 02. This work was partially funded by Spanish MCIN/AEI/ 10.13039/501100011033 under Grants No. RTI2018-098868-B-I00 and No. PID2021-126998OB-I00, and by Grupo de Física Nuclear (910059) at Universidad Complutense de Madrid. This work was supported by German BMBF under contract 05P21PKCI1 and Verbundprojekt 05P2021. This work was supported by the Generalitat Valenciana PROMETEO CIPROM/2022/9 project and by the Ministerio de Ciencia e Innovación Grant PID2022-138297NB-C21; also the Centro de Excelencia Severo Ochoa CEX2023-001292-S grant funded by MCIU/AEI is acknowledged.

This work was supported by the Fonds de la Recherche Scientifique (F.R.S.-FNRS) and the Fonds Wetenschappelijk Onderzoek - Vlaanderen (FWO) under the EOS Project nr O022818F, IRI Project I002619N and IRI Project I001323N, by GOA/2015/010 and C14/22/104 (BOF KU Leuven), the Interuniversity Attraction Poles Programme initiated by the Belgian Science Policy Office (BriX network P7/12), by the ENSAR2: European Union's Horizon 2020 research and innovation programme under grant agreement No 654002, by the U.K. Science and Technology Facilities Council through Grant Nos. ST/P004598/1, ST/V001027/1, ST/Y000285/1 and ST/Y000242/1, by the Slovak Research and Development Agency (Contract No. APVV-22-0282), by the Slovak grant agency VEGA (Contract No. 1/0019/25); by the Max Planck Society, the German Federal Ministry of Education and Research (BMBF) (Grants No. 05P12HGCI1, No. 05P12HGFNE, and No. 05P15ODCIA) and by the French IN2P3.

References

[1] D.T. Yordanov, D.L. Balabanski, J. Bieroń, M.L. Bissell, K. Blaum, I.B. Čević, S. Fritzsche, N. Frömmgen, G. Georgiev, C. Geppert, M. Hammen, M. Kowalska, K. Kreim, A. Krieger, R. Neugart, W. Nörtershäuser, J. Papuga, S. Schmidt, Spins, electromagnetic moments, and isomers of $^{107-129}$Cd, Phys. Rev. Lett. 110 (2013) 192501. https://doi.org/10.1103/PhysRevLett.110.192501

[2] R.D. Groote, D. Nesterenko, A. Kankainen, M. Bissell, O. Beliuskina, J. Bonnard, P. Campbell, L. Canete, B. Cheal, C. Delafosse, A.D. Roubin, C. Devlin, J. Dobaczewski, T. Eronen, R.G. Ruiz, S. Geldhof, W. Gins, M. Hukkanen, P. Imgram, R. Mathieson, A. Koszorús, I. Moore, I. Pohjalainen, M. Reponen, B.V.D. Borne, M. Vilén, S. Zadvornaya, Measurements of binding energies and electromagnetic moments of silver isotopes: a complementary benchmark of density functional theory, Phys. Lett. B 848 (2024) 138352. https://doi.org/10.1016/j.physletb.2023.138352

[3] Z. Yue, A. Andreyev, A. Barzakh, I. Borzov, J. Cubiss, A. Algora, M. Au, M. Balogh, S. Bara, R. Bark, C. Bernerd, M. Borge, D. Brugnara, K. Chrysalidis, T. Cocolios, H.D. Witte, Z. Favier, L. Fraile, H. Fynbo, A. Gottardo, R. Grzywacz, R. Heinke, A. Illana, P. Jones, D. Judson, A. Korgul, U. Köster, M. Labiche, L. Le, R. Lica, M. Madurga, N. Marginean, B. Marsh, C. Mihai, E. Nácher, C. Neacsu, C. Nita, B. Olaizola, J. Orce, C. Page, R. Page, J. Pakarinen, P. Papadakis, G. Penyazkov, A. Perea, M.P.-S. kowska, Z. Podolyák, S. Prosnyak, E. Reis, S. Rothe, M. Sedlak, L. Skripnikov, C. Sotty, S. Stegemann, O. Tengblad, S. Tolokonnikov, J. Udías, P.V. Duppen, N. Warr, W. Wojtaczka, Magnetic moments of thallium isotopes in the vicinity of magic $N = 126$, Phys. Lett. B 849 (2024) 138452. https://doi.org/10.1016/j.physletb.2024.138452

[4] P.L. Sassarini, J. Dobaczewski, J. Bonnard, R.F.G. Ruiz, Nuclear DFT analysis of electromagnetic moments in odd near doubly magic nuclei, J. Phys. G 49 (11) (2022). https://doi.org/10.1088/1361-6471/ac900a

[5] J. Bonnard, J. Dobaczewski, G. Danneaux, M. Kortelainen, Nuclear DFT electromagnetic moments in heavy deformed open-shell odd nuclei, Phys. Lett. B 843 (2023) 138014. https://doi.org/10.1016/j.physletb.2023.138014

[6] S.A. Ahmad, W. Klempt, C. Ekström, R. Neugart, K. Wendt, Nuclear spins, moments, and changes of the mean square charge radii of 140-153Eu, Z. Phys. A 321 (1985) 35. https://doi.org/10.1007/BF01411941

[7] R. Neugart, H.H. Stroke, S.A. Ahmad, H.T. Duong, H.L. Ravn, K. Wendt, Nuclear magnetic moment of ^{207}Tl, Phys. Rev. Lett. 55 (1985) 1559–1562. https://doi.org/10.1103/PhysRevLett.55.1559

[8] A.R. Vernon, R.F.G. Ruiz, T. Miyagi, C.L. Binnersley, J. Billowes, M.L. Bissell, J. Bonnard, T.E. Cocolios, J. Dobaczewski, G.J. Farooq-Smith, K.T. Flanagan, G. Georgiev, W. Gins, R.P.D. Groote, R. Heinke, J.D. Holt, J. Hustings, A. Koszorús, D. Leimbach, K.M. Lynch, G. Neyens, S.R. Stroberg, S.G. Wilkins, X.F. Yang, D.T. Yordanov, Nuclear moments of indium isotopes reveal abrupt change at magic number 82, Nature 607 (2022) 260. https://doi.org/10.1038/s41586-022-04818-7

[9] S. Schmidt, J. Billowes, M. Bissell, K. Blaum, R.G. Ruiz, H. Heylen, S. Malbrunot-Ettenauer, G. Neyens, W. Nörtershäuser, G. Plunien, S. Sailer, V. Shabaev, L. Skripnikov, I. Tupitsyn, A. Volotka, X. Yang, The nuclear magnetic moment of 208Bi and its relevance for a test of bound-state strong-field QED, Phys. Lett. B 779 (2018) 324–330. https://www.sciencedirect.com/science/article/pii/S0370269318301266.

[10] J.G. Cubiss, A.E. Barzakh, M.D. Seliverstov, A.N. Andreyev, B. Andel, S. Antalic, P. Ascher, D. Atanasov, D. Beck, J.B. Ń, K. Blaum, C. Borgmann, M. Breitenfeldt, L. Capponi, T.E. Cocolios, T.D. Goodacre, X. Derkx, H.D. Witte, J. Elseviers, D.V. Fedorov, V.N. Fedosseev, S. Fritzsche, L.P. Gaffney, S. George, L. Ghys, F.P. Heßberger, M. Huyse, N. Imai, Z. Kalaninová, D. Kisler, U. Köster, M. Kowalska, S. Kreim, J.F.W. Lane, V. Liberati, D. Lunney, K.M. Lynch, V. Manea, B.A. Marsh, S. Mitsuoka, P.L. Molkanov, Y. Nagame, D. Neidherr, K. Nishio, S. Ota, D. Pauwels, L. Popescu, D. Radulov, E. Rapisarda, J.P. Revill, M. Rosenbusch, R.E. Rossel, S. Rothe, K. Sandhu, L. Schweikhard, S. Sels, V.L. Truesdale, C.V. Beveren, P.V.D. Bergh, Y. Wakabayashi, P.V. Duppen, K.D.A. Wendt, F. Wienholtz, B.W. Whitmore, G.L. Wilson, R.N. Wolf, K. Zuber, Charge radii and electromagnetic moments of $^{195-211}$At, Phys. Rev. C 97 (2018) 54327. https://doi.org/10.1103/PhysRevC.97.054327

[11] H. Wibowo, B.C. Backes, J. Dobaczewski, R.P.D. Groote, A. Nagpal, A. Sánchez-Fernández, X. Sun, J.L. Wood, Electromagnetic moments in the Sn-Gd region de-

termined within nuclear DFT, J. Phys. G 52 (6) (2025) 65104. https://doi.org/10.1088/1361-6471/ade0dd
[12] M.R. Pearson, P. Campbell, K. Leerungnavarat, J. Billowes, I.S. Grant, M. Keim, J. Kilgallon, I.D. Moore, R. Neugart, M. Neuroth, S. Wilbert, Nuclear moments and charge radii of bismuth isotopes, J. Phys. G 26 (12) (2000) 1829–1848. https://doi.org/10.1088/2F0954-3899/2F26/2F12/2F307
[13] A.E. Barzakh, D.V. Fedorov, V.S. Ivanov, P.L. Molkanov, F.V. Moroz, S.Y. Orlov, V.N. Panteleev, M.D. Seliverstov, Y.M. Volkov, Onset of deformation in neutron-deficient Bi isotopes studied by laser spectroscopy, Phys. Rev. C 95 (2017) 44324. https://doi.org/10.1103/PhysRevC.95.044324
[14] A.E. Barzakh, D.V. Fedorov, V.S. Ivanov, P.L. Molkanov, F.V. Moroz, S.Y. Orlov, V.N. Panteleev, M.D. Seliverstov, Y.M. Volkov, Shell effect in the mean square charge radii and magnetic moments of bismuth isotopes near $N = 126$, Phys. Rev. C 97 (2018) 14322. https://doi.org/10.1103/PhysRevC.97.014322
[15] I.N. Borzov, E.E. Saperstein, S.V. Tolokonnikov, Magnetic moments of spherical nuclei: Status of the problem and unsolved issues, Phys. At. Nucl. 71 (3) (2008) 469. https://doi.org/10.1134/S1063778808030095
[16] I.N. Borzov, E.E. Saperstein, S.V. Tolokonnikov, G. Neyens, N. Severijns, Description of magnetic moments of long isotopic chains within the FFS theory, Eur. Phys. J. A 45 (2010) 159. https://doi.org/10.1140/epja/i2010-10985-y
[17] E.E. Saperstein, O.I. Achakovskiy, S.P. Kamerdzhiev, S. Krewald, J. Speth, S.V. Tolokonnikov, Phonon coupling effects in magnetic moments of magic and semimagic nuclei, Phys. Atom. Nucl. 77 (2014) 1033. https://doi.org/10.1134/S1063778814080122
[18] O.I. Achakovskiy, S.P. Kamerdzhiev, E.E. Saperstein, S.V. Tolokonnikov, Magnetic moments of odd-odd spherical nuclei, Eur. Phys. J. A 50 (2014) 6. https://doi.org/10.1140/epja/i2014-14006-1
[19] M. Liu, C. Yuan, Recent progress in configuration-interaction shell model, Int. J. Mod. Phys. E 32 (12) (2023) 2330003. https://doi.org/10.1142/S0218301323300035
[20] C. Yuan, M. Liu, N. Shimizu, Z. Podolyák, T. Suzuki, T. Otsuka, Z. Liu, Shell-model study on spectroscopic properties in the region "south" of ^{208}Pb, Phys. Rev. C 106 (2022) 44314. https://doi.org/10.1103/PhysRevC.106.044314
[21] T.T. Yeung, A.I. Morales, J. Wu, M. Liu, C. Yuan, S. Nishimura, V.H. Phong, N. Fukuda, J.L. Tain, T. Davinson, K.P. Rykaczewski, R. Yokoyama, T. Isobe, M. Niikura, Z. Podolyák, G. Alcalá, A. Algora, J.M. Allmond, J. Agramunt, C. Appleton, H. Baba, R. Caballero-Folch, F. Calvino, M.P. Carpenter, I. Dillmann, A. Estrade, T. Gao, C.J. Griffin, R.K. Grzywacz, O. Hall, Y. Hirayama, B.M. Hue, E. Ideguchi, G.G. Kiss, K. Kokubun, F.G. Kondev, R. Mizuno, M. Mukai, N. Nepal, M.N. Nurhafiza, S. Ohta, S.E.A. Orrigo, M. Pallàs, J. Park, B.C. Rasco, D.R. ǵuez Garcı á, H. Sakurai, L. Sexton, Y. Shimizu, H. Suzuki, A. Vitéz-Sveiczer, H. Takeda, A. Tarifeno-Saldivia, A. Tolosa-Delgado, J.A. Victoria, Y.X. Watanabe, J.M. Yap, First exploration of monopole-driven shell evolution above the $N = 126$ shell closure: New millisecond isomers in ^{213}Tl and ^{215}Tl, Phys. Rev. Lett. 133 (2024) 72501. https://doi.org/10.1103/PhysRevLett.133.072501
[22] P.C. Srivastava, S. Sharma, A. Kumar, P. Choudhary, Shell model study of first-forbidden beta decay around 208Pb, J. Phys.: Conf. Ser. 2586 (1) (2023) 12026. https://doi.org/10.1088/1742-6596/2586/1/012026
[23] H. Naïdja, New shell-model investigation of the 208Pb mass region, Phys. Scr. 94 (1) (2018) 14005. https://doi.org/10.1088/1402-4896/aaeca4
[24] B. Andel, P.V. Duppen, A.N. Andreyev, A. Blazhev, H. Grawe, R. Licăă, H.N. d̈ja, M. Stryjczyk, A. Algora, S. Antalic, A. Barzakh, J. Benito, G. Benzoni, T. Berry, M.J.G. Borge, K. Chrysalidis, C. Clisu, C. Costache, J.G. Cubiss, H.D. Witte, D.V. Fedorov, V.N. Fedosseev, L.M. Fraile, H.O.U. Fynbo, P.T. Greenlees, L.J. Harkness-Brennan, M. Huyse, A. Illana, J. Jolie, D.S. Judson, J. Konki, I. Lazarus, M. Madurga, N. Marginean, R. Marginean, C. Mihai, B.A. Marsh, P. Molkanov, P. Mosat, J.R. Murias, E. Nacher, A. Negret, R.D. Page, S. Pascu, A. Perea, V. Pucknell, P. Rahkila, E. Rapisarda, K. Rezynkina, V. Sánchez-Tembleque, K. Schomacker, M.D. Seliverstov, C. Sotty, L. Stan, C. Sürder, O. Tengblad, V. Vedia, S.V. Nals, R. Wadsworth, N. Warr, New β-decaying state in ^{214}Bi, Phys. Rev. C 104 (2021) 54301. https://doi.org/10.1103/PhysRevC.104.054301
[25] B. Andel, A.N. Andreyev, A. Blazhev, R. Licăă, H.N. d̈ja, M. Stryjczyk, P.V. Duppen, A. Algora, S. Antalic, A. Barzakh, J. Benito, G. Benzoni, T. Berry, M.J.G. Borge, K. Chrysalidis, C. Clisu, C. Costache, J.G. Cubiss, H.D. Witte, D.V. Fedorov, V.N. Fedosseev, L.M. Fraile, H.O.U. Fynbo, P.T. Greenlees, L.J. Harkness-Brennan, M. Huyse, A. Illana, J. Jolie, D.S. Judson, J. Konki, I. Lazarus, M. Madurga, N. Marginean, R. Marginean, B.A. Marsh, C. Mihai, P.L. Molkanov, P. Mosat, J.R. Murias, E. Nacher, A. Negret, R.D. Page, S. Pascu, A. Perea, V. Pucknell, P. Rahkila, E. Rapisarda, K. Rezynkina, V. Sánchez-Tembleque, K. Schomacker, M.D. Seliverstov, C. Sotty, L. Stan, C. Sürder, O. Tengblad, V. Vedia, S.V. Nals, R. Wadsworth, N. Warr, β decay of the ground state and of a low-lying isomer in ^{216}Bi, Phys. Rev. C 109 (2024) 64321. https://doi.org/10.1103/PhysRevC.109.064321
[26] T. Otsuka, T. Suzuki, M. Honma, Y. Utsuno, N. Tsunoda, K. Tsukiyama, M. Hjorth-Jensen, Novel features of nuclear forces and shell evolution in exotic nuclei, Phys. Rev. Lett. 104 (2010) 12501. https://doi.org/10.1103/PhysRevLett.104.012501
[27] C. Yuan, M. Liu, Y. Ge, Shell-model explanation on some newly discovered isomers, Nucl. Phys. Rev. 37 (3) (2020) 447–454. https://doi.org/10.11804/NuclPhysRev.37.2019CNPC18
[28] R. Catherall, W. Andreazza, M. Breitenfeldt, A. Dorsival, G.J. Focker, T.P. Gharsa, T.J. G, J.-L. Grenard, F. Locci, P. Martins, S. Marzari, J. Schipper, A. Shornikov, T. Stora, The ISOLDE facility, J. Phys. G 44 (9) (2017) 94002. https://doi.org/10.1088/2F1361-6471/2Faa7eba
[29] V. Fedosseev, K. Chrysalidis, T.D. Goodacre, B. Marsh, S. Rothe, C. Seiffert, K. Wendt, Ion beam production and study of radioactive isotopes with the laser ion source at ISOLDE, J. Phys. G 44 (8) 2017–084006. https://doi.org/10.1088/2F1361-6471/2Faa78e0
[30] S. Rothe, T.D. Goodacre, D. Fedorov, V. Fedosseev, B. Marsh, P. Molkanov, R. Rossel, M. Seliverstov, M. Veinhard, K. Wendt, Laser ion beam production at CERN-ISOLDE: New features - More possibilities, Nucl. Instrum. Methods Phys. Res., Sect. B 376 (2016) 91–96. https://www.sciencedirect.com/science/article/pii/S0168583X1600152X.
[31] M. Seliverstov, A. Barzakh, R. Ahmed, K. Chrysalidis, T.D. Goodacre, D. Fedorov, V. Fedoseev, C. Granados, B. Marsh, P. Molkanov, V. Panteleev, R.E. Rossel, S. Rothe, S. Wilkins, IS608 Collaboration, In-source laser photoionization spectroscopy of Bi isotopes: accuracy of the technique and methods of data analysis, Hyperfine Interact. 241 (1) (2020) 40. https://doi.org/10.1007/s10751-020-01710-6
[32] S. Rothe, V. Fedosseev, T. Kron, B. Marsh, R. Rossel, K. Wendt, Narrow linewidth operation of the rilis titanium: Sapphire laser at ISOLDE/CERN, Nucl. Instrum. Methods Phys. Res., Sect. B 317 (2013) 561–564. https://doi.org/10.1016/j.nimb.2013.08.058
[33] R. Wolf, F. Wienholtz, D. Atanasov, D. Beck, K. Blaum, C. Borgmann, F. Herfurth, M. Kowalska, S. Kreim, Y.A. Litvinov, D. Lunney, V. Manea, D. Neidherr, M. Rosenbusch, L. Schweikhard, J. Stanja, K. Zuber, Isoltrap's multi-reflection time-of-flight mass separator/spectrometer, 2013, pp. 123–133. https://doi.org/10.1016/j.ijms.2013.03.020
[34] A.E. Barzakh, D. Atanasov, A.N. Andreyev, M.A. Monthery, N.A. Althubiti, B. Andel, S. Antalic, K. Blaum, T.E. Cocolios, J.G. Cubiss, P.V. Duppen, T.D. Goodacre, A.D. Roubin, G.J. Farooq-Smith, D.V. Fedorov, V.N. Fedosseev, D.A. Fink, L.P. Gaffney, L. Ghys, R.D. Harding, M. Huyse, N. Imai, S. Kreim, D. Lunney, K.M. Lynch, V. Manea, B.A. Marsh, Y.M. Palenzuela, P.L. Molkanov, D. Neidherr, M. Rosenbusch, R.E. Rossel, S. Rothe, L. Schweikhard, M.D. Seliverstov, S. Sels, C.V. Beveren, E. Verstraelen, A. Welker, F. Wienholtz, R.N. Wolf, K. Zuber, Shape coexistence in ^{187}Au studied by laser spectroscopy, Phys. Rev. C 101 (2020) 64321. https://doi.org/10.1103/PhysRevC.101.064321
[35] I. D. Station, 04.05.2025, https://isolde-ids.web.cern.ch/.
[36] A. Barzakh, A.N. Andreyev, C. Raison, J.G. Cubiss, P.V. Duppen, S. Péru, S. Hilaire, S. Goriely, B. Andel, S. Antalic, M.A. Monthery, J.C. Berengut, J. Bieroń, M.L. Bissell, A. Borschevsky, K. Chrysalidis, T.E. Cocolios, T.D. Goodacre, J.-P. Dognon, M. Elantkowska, E. Eliav, G.J. Farooq-Smith, D.V. Fedorov, V.N. Fedosseev, L.P. Gaffney, R.F.G. Ruiz, M. Godefroid, C. Granados, R.D. Harding, R. Heinke, M. Huyse, J. Karls, P. Larmonier, J.G. Li, K.M. Lynch, D.E. Maison, B.A. Marsh, P. Molkanov, P. Mosat, A.V. Oleynichenko, V. Panteleev, P. Pyykkö, M.L. Reitsma, K. Rezynkina, R.E. Rossel, S. Rothe, J. Ruczkowski, S. Schiffmann, C. Seiffert, M.D. Seliverstov, S. Sels, L.V. Skripnikov, M. Stryjczyk, D. Studer, M. Verlinde, S. Wilman, A.V. Zaitsevskii, Large shape staggering in neutron-deficient Bi isotopes, Phys. Rev. Lett. 127 (2021) 192501. https://doi.org/10.1103/PhysRevLett.127.192501
[37] E. W. Otten, Nuclear radii and moments of unstable isotopes, in: D. A. Bromley, (Ed.), Treatise on Heavy Ion Science: Volume 8: Nuclear Far From Stability, Springer, Boston, MA, 1989, pp. 517–638.
[38] A.I. Morales, G. Benzoni, A. Gottardo, J.J. Valiente-Dobón, N. Blasi, A. Bracco, F. Camera, F.C.L. Crespi, A. Corsi, S. Leoni, B. Million, R. Nicolini, O. Wieland, A. Gadea, S. Lunardi, M. Górska, P.H. Regan, Z. Podolyák, M. Pfützner, S. Pietri, P. Boutachkov, H. Weick, J. Grebosz, A.M. Bruce, J.A.N. Nez, A. Algora, N. Al-Dahan, Y. Ayyad, N. Alkhomashi, P.R.P. Allegro, D. Bazzacco, J. Benlliure, M. Bowry, M. Bunce, E. Casarejos, M.L. Cortes, A.M.D. Bacelar, A.Y. Deo, G.D. Angelis, C. Domingo-Pardo, M. Doncel, Z. Dombradi, T. Engert, K. Eppinger, G.F. Farrelly, F. Farinon, E. Farnea, H. Geissel, J. Gerl, N. Goel, E. Gregor, T. Habermann, R. Hoischen, R. Janik, S. Klupp, I. Kojouharov, N. Kurz, S. Mandal, R. Menegazzo, D. Mengoni, D.R. Napoli, F. Naqvi, β-decay studies of neutron-rich Tl, Pb, and Bi isotopes, Phys. Rev. C 89 (2014) 14324. https://doi.org/10.1103/PhysRevC.89.014324
[39] J. Kurpeta, A.P. ochocki, A. Andreyev, J. Äystö, A. De, H.D. Smet, A.-H. Witte, V. Evensen, S. Fedoseyev, M. Franchoo, H. Górska, M. Grawe, M. Huhta, Z. Huyse, A. Janas, M. Jokinen, E. Karny, U. Kugler, W. Kurcewicz, J. Köster, A. Lettry, K. Nieminen, M. Partes, H. Ramdhane, K. Ravn, J. Rykaczewski, K. Szerypo, P.V.D. Vel, L.V. Duppen, G. Weissman, A. Walter, W. Collaboration, T.I. Collaboration, Isomeric and ground-state decay of ^{215}PLXBi, Eur. Phys. J. A 18 (1) (2003) 31. https://doi.org/10.1140/epja/i2003-10066-6
[40] J. Kurpeta, A.P. ochocki, A. Andreyev, J. Äystö, A. De, H.D. Smet, A.-H. Witte, V. Evensen, S. Fedoseyev, M. Franchoo, M. Górska, M. Huhta, Z. Huyse, A. Janas, M. Jokinen, E. Karny, U. Kugler, W. Kurcewicz, J. Köster, A. Lettry, K. Nieminen, M. Partes, H. Ramdhane, K. Ravn, J. Rykaczewski, K. Szerypo, P.V.D. Vel, L.V. Duppen, G. Weissman, A. Walter, W. Collaboration, T.I. Collaboration, The decay of the new neutron-rich isotope ^{217}Bi, Eur. Phys. J. A 18 (1) (2003) 5. https://doi.org/10.1140/epja/i2003-10065-7
[41] A. Gottardo, J.J. Valiente-Dobón, G. Benzoni, S. Lunardi, A. Gadea, A. Algora, N. Al-Dahan, G.D. Angelis, Y. Ayyad, D. Bazzacco, J. Benlliure, P. Boutachkov, M. Bowry, A. Bracco, A.M. Bruce, M. Bunce, F. Camera, E. Casarejos, M.L. Cortes, F.C.L. Crespi, A. Corsi, A.M.D. Bacelar, A.Y. Deo, C. Domingo-Pardo, M. Doncel, T. Engert, K. Eppinger, G.F. Farrelly, F. Farinon, E. Farnea, H. Geissel, J. Gerl, N. Goel, M. Górska, J. Grebosz, E. Gregor, T. Habermann, R. Hoischen, R. Janik, P.R. John, S. Klupp, I. Kojouharov, N. Kurz, S.M. Lenzi, S. Leoni, S. Mandal, R. Menegazzo, D. Mengoni, B. Million, V. Modamio, A.I. Morales, D.R. Napoli, F. Naqvi, R. Nicolini, C. Nociforo, M. Pfützner, S. Pietri, Z. Podolyák, A. Prochazka, W. Prokopowicz, F. Recchia, P.H. Regan, M.W. Reed, D. Rudolph, E. Sahin, H. Schaffner, A. Sharma, B. Sitar, D. Siwal, K. Steiger, P. Strmen, T.P.D. Swan, I. Szarka, C.A. Ur, P.M. Walker, H. Weick, O. Wieland, H.-J. Wollersheim, Isomeric decay spectroscopy of the ^{217}Bi isotope, Phys. Rev. C 90 (2014) 34317. https://doi.org/10.1103/PhysRevC.90.034317
[42] R.J. Hull, G.O. Brink, Hyperfine structure of Bi^{209}, Phys. Rev. A 1 (1970) 685–693. https://doi.org/10.1103/PhysRevA.1.685
[43] M. Bissel, 2024. Unpublished.
[44] M. Basunia, Nuclear data sheets for A = 213, Nuclear Data Sheets 181 (2022) 475–585. https://doi.org/10.1016/j.nds.2022.03.002

[45] B. Singh, G. Mukherjee, D. Abriola, S.K. Basu, P. Demetriou, A. Jain, S. Kumar, S. Singh, J. Tuli, Nuclear data sheets for A = 215, Nuclear Data Sheets 114 (12) (2013) 2023–2078. https://doi.org/10.1016/j.nds.2013.11.003

[46] E. Browne, Nuclear data sheets for A = 215, Nucl. Data Sheets 219 (4) (2001) 763–1061. https://doi.org/10.1006/ndsh.2001.0016

[47] A.K. Jain, S. Singh, S. Kumar, J.K. Tuli, Nuclear data sheets for A = 221, Nucl. Data Sheets 108 (4) (2007) 883–922. https://doi.org/10.1016/j.nds.2007.03.002

[48] A.E. Barzakh, J.G. Cubiss, A.N. Andreyev, M.D. Seliverstov, B. Andel, S. Antalic, P. Ascher, D. Atanasov, D. Beck, J.B. Ń, K. Blaum, C. Borgmann, M. Breitenfeldt, L. Capponi, T.E. Cocolios, T.D. Goodacre, X. Derkx, H.D. Witte, J. Elseviers, D.V. Fedorov, V.N. Fedosseev, S. Fritzsche, L.P. Gaffney, S. George, L. Ghys, F.P. Heßberger, M. Huyse, N. Imai, Z. Kalaninová, D. Kisler, U. Köster, M. Kowalska, S. Kreim, J.F.W. Lane, V. Liberati, D. Lunney, K.M. Lynch, V. Manea, B.A. Marsh, S. Mitsuoka, P.L. Molkanov, Y. Nagame, D. Neidherr, K. Nishio, S. Ota, D. Pauwels, L. Popescu, D. Radulov, E. Rapisarda, J.P. Revill, M. Rosenbusch, R.E. Rossel, S. Rothe, K. Sandhu, L. Schweikhard, S. Sels, V.L. Truesdale, C.V. Beveren, P.V.D. Bergh, P.V. Duppen, Y. Wakabayashi, K.D.A. Wendt, F. Wienholtz, B.W. Whitmore, G.L. Wilson, R.N. Wolf, K. Zuber, Inverse odd-even staggering in nuclear charge radii and possible octupole collectivity in ^{217,218,219}At revealed by in-source laser spectroscopy, Phys. Rev. C 99 (2019) 54317. https://doi.org/10.1103/PhysRevC.99.054317

[49] A. Coc, C. Thibault, F. Touchard, H. Duong, P. Juncar, S. Liberman, J. Pinard, J. Lermé, J. Vialle, S. Büttgenbach, A. Mueller, A. Pesnelle, Hyperfine structures and isotope shifts of 207-213,220-228Fr; possible evidence of octupolar deformation, Phys. Lett. B 163 (1) (1985) 66–70. https://doi.org/10.1016/0370-2693(85)90193-5

[50] R.P.D. Groote, I.B. Čević, J. Billowes, M.L. Bissell, T.E. Cocolios, G.J. Farooq-Smith, V.N. Fedosseev, K.T. Flanagan, S. Franchoo, R.F.G. Ruiz, H. Heylen, R. Li, K.M. Lynch, B.A. Marsh, G. Neyens, R.E. Rossel, S. Rothe, H.H. Stroke, K.D.A. Wendt, S.G. Wilkins, X. Yang, Use of a continuous wave laser and pockels cell for sensitive high-resolution collinear resonance ionization spectroscopy, Phys. Rev. Lett. 115 (2015) 132501. https://doi.org/10.1103/PhysRevLett.115.132501

[51] C.F. Liang, P. Paris, R.K. Sheline, α decay of ^{223}Fr : level structure of ^{219}At, Phys. Rev. C 64 (2001) 34310. https://doi.org/10.1103/PhysRevC.64.034310

[52] C.F. Liang, P. Paris, J. Kvasil, R.K. Sheline, ^{219}Fr, a transitional reflection asymmetric nucleus, Phys. Rev. C 44 (1991) 676–688. https://doi.org/10.1103/PhysRevC.44.676

[53] C. Liang, A. Péghaire, R. Sheline, Octupole deformation in ^{221}Fr; E1 transitional rates, Modern Phys. Lett. A 05 (16) (1990). https://doi.org/10.1142/S0217732390001402

[54] I. Budinčevi, J. Billowes, M.L. Bissell, T.E. Cocolios, R.P.D. Groote, S.D. Schepper, V.N. Fedosseev, K.T. Flanagan, S. Franchoo, R.F.G. Ruiz, H. Heylen, K.M. Lynch, B.A. Marsh, G. Neyens, T.J. Procter, R.E. Rossel, S. Rothe, I. Strashnov, H.H. Stroke, K.D.A. Wendt, Laser spectroscopy of francium isotopes at the borders of the region of reflection asymmetry, Phys. Rev. C 90 (2014) 14317. https://doi.org/10.1103/PhysRevC.90.014317

[55] A. Barzakh, A.N. Andreyev, Z. Yue, L. Nies, M.D. Seliverstov, J.G. Cubiss, A. Algora, B. Andel, S. Antalic, M.A. Monthery, D. Atanasov, J. Benito, G. Benzoni, T. Berry, M.L. Bissell, K. Blaum, M.J.G. Borge, K. Chrysalidis, C. Clisu, T.E. Cocolios, C. Costache, T.D. Goodacre, G.J. Farooq-Smith, D.V. Fedorov, V.N. Fedosseev, L.M. Fraile, H.O.U. Fynbo, V. Gadelshin, L.P. Gaffney, R.F.G. Ruiz, C. Granados, P.T. Greenlees, R.D. Harding, L.J. Harkness-Brennan, R. Heinke, A. Herlert, M. Huyse, A. Illana, J. Jolie, D.S. Judson, J. Karls, J. Konki, P. Larmonier, I. Lazarus, D. Leimbach, R. Licăă, Z. Liu, D. Lunney, K.M. Lynch, M. Madurga, V. Manea, N. Marginean, R. Marginean, B.A. Marsh, C. Mihai, P. Molkanov, P. Mosat, M. Mougeot, J.R. Murias, E. Nacher, A. Negret, D. Neidherr, R.D. Page, S. Pascu, A. Perea, V. Pucknell, P. Rahkila, C. Raison, E. Rapisarda, K. Rezynkina, M. Rosenbush, R.E. Rossel, S. Rothe, V. Sánchez-Tembleque, K. Schomacker, L. Schweikhard, C. Seiffert, S. Sels, C. Sotty, L. Stan, M. Stryjczyk, D. Studer, J. Sundberg, C. Sürder, O. Tengblad, P.V. Duppen, V. Vedia, M. Verlinde, S.V. Nals, N. Warr, A. Welker, F. Wienholtz, R.N. Wolf, Charge radii and electromagnetic moments of $^{214-218}$Bi: Exploring the "southern" border of the $Z > 82$ octupole-deformation region, Phys. Rev. C 112 (2025) 34304. https://doi.org/10.1103/sltw-g4d6

[56] W.A. Richter, S. Mkhize, B.A. Brown, *sd*-shell observables for the usda and usdb hamiltonians, Phys. Rev. C 78 (2008) 64302. https://doi.org/10.1103/PhysRevC.78.064302

[57] H. Hübel, Kernstrukturaussagen magnetischer momente von hochspinzuständen, Fortschritte der Physik 25 (1977) 327–371. https://doi.org/10.1002/prop.19770250110

[58] T. Yamazaki, Mesonic exchange effect on nuclear magnetic moments and related problems - experimental, Mesons in Nuclei II (1979) 652.

[59] G. Neyens, Nuclear magnetic and quadrupole moments for nuclear structure research on exotic nuclei, Reports on Progress in Physics 66 (4) (2003) 633. https://doi.org/10.1088/0034-4885/66/4/205

[60] E. Caurier, G.M. ńez Pinedo, F. Nowacki, A. Poves, A.P. Zuker, The shell model as a unified view of nuclear structure, Rev. Mod. Phys. 77 (2005) 427–488. https://doi.org/10.1103/RevModPhys.77.427

[61] G. Fu, C.W. Johnson, From deformed Hartree-Fock to the nucleon-pair approximation, Phys. Lett. B 809 (2020) 135705. https://doi.org/10.1016/j.physletb.2020.135705

[62] N. Shimizu, T. Mizusaki, Y. Utsuno, Y. Tsunoda, Thick-restart block lanczos method for large-scale shell-model calculations, Comput. Phys. Commun. 244 (2019) 372–384. https://doi.org/10.1016/j.cpc.2019.06.011

[63] J. Chen, M. Liu, C. Yuan, S. Chen, N. Shimizu, X. Sun, R. Xu, Y. Tian, Shell-model-based investigation on level density of Xe and Ba isotopes, Phys. Rev. C 107 (2023) 54306. https://doi.org/10.1103/PhysRevC.107.054306

[64] T. Otsuka, Emerging concepts in nuclear structure based on the shell model, Physics 4 (1) (2022) 258–285. https://doi.org/10.3390/physics4010018

[65] G. Bertsch, J. Borysowicz, H. Mcmanus, W. Love, Interactions for inelastic scattering derived from realistic potentials, Nucl. Phys. A 284 (3) (1977) 399–419. https://doi.org/10.1016/0375-9474(77)90392-X.

[66] C. Yuan, Ge, Yulin, Liu, Menglan, Chen, Guangshang, B. Cai, Recent shell-model investigation and its possible role in nuclear structure data study,, EPJ Web Conf. 239 (2020) 4002. https://doi.org/10.1051/epjconf/202023904002

[67] E.K. Warburton, B.A. Brown, Appraisal of the kuo-herling shell-model interaction and application to A=210-212 nuclei, Phys. Rev. C 43 (1991) 602–617. https://doi.org/10.1103/PhysRevC.43.602

[68] E.K. Warburton, First-forbidden β decay in the lead region and mesonic enhancement of the weak axial current, Phys. Rev. C 44 (1991) 233–260. https://doi.org/10.1103/PhysRevC.44.233

[69] Z.Y. Zhang, H.B. Yang, M.H. Huang, Z.G. Gan, C.X. Yuan, C. Qi, A.N. Andreyev, M.L. Liu, L. Ma, M.M. Zhang, Y.L. Tian, Y.S. Wang, J.G. Wang, C.L. Yang, G.S. Li, Y.H. Qiang, W.Q. Yang, R.F. Chen, H.B. Zhang, Z.W. Lu, X.X. Xu, L.M. Duan, H.R. Yang, W.X. Huang, Z. Liu, X.H. Zhou, Y.H. Zhang, H.S. Xu, N. Wang, H.B. Zhou, X.J. Wen, S. Huang, W. Hua, L. Zhu, X. Wang, Y.C. Mao, X.T. He, S.Y. Wang, W.Z. Xu, H.W. Li, Z.Z. Ren, S.G. Zhou, New α-emitting isotope ^{214}U and abnormal enhancement of α-particle clustering in lightest uranium isotopes, Phys. Rev. Lett. 126 (2021) 152502. https://doi.org/10.1103/PhysRevLett.126.152502

[70] P.M. Goddard, P.D. Stevenson, A. Rios, Charge radius isotope shift across the $N = 126$ shell gap, Phys. Rev. Lett. 110 (2013) 32503. https://doi.org/10.1103/PhysRevLett.110.032503

[71] T.D. Goodacre, A.V. Afanasjev, A.E. Barzakh, B.A. Marsh, S. Sels, P. Ring, H. Nakada, A.N. Andreyev, P.V. Duppen, N.A. Althubiti, B. Andel, D. Atanasov, J. Billowes, K. Blaum, T.E. Cocolios, J.G. Cubiss, G.J. Farooq-Smith, D.V. Fedorov, V.N. Fedosseev, K.T. Flanagan, L.P. Gaffney, L. Ghys, M. Huyse, S. Kreim, D. Lunney, K.M. Lynch, V. Manea, Y.M. Palenzuela, P.L. Molkanov, M. Rosenbusch, R.E. Rossel, S. Rothe, L. Schweikhard, M.D. Seliverstov, P. Spagnoletti, C.V. Beveren, M. Veinhard, E. Verstraelen, A. Welker, K. Wendt, F. Wienholtz, R.N. Wolf, A. Zadvornaya, K. Zuber, Laser spectroscopy of neutron-rich ^{207,208}Hg isotopes: illuminating the kink and odd-even staggering in charge radii across the $N = 126$ shell closure, Phys. Rev. Lett. 126 (2021) 32502. https://doi.org/10.1103/PhysRevLett.126.032502

[72] U.C. Perera, A.V. Afanasjev, P. Ring, Charge radii in covariant density functional theory: A global view, Phys. Rev. C 104 (2021) 64313. https://doi.org/10.1103/PhysRevC.104.064313

[73] Z. Yue, A.E. Barzakh, A.N. Andreyev, I.N. Borzov, J.G. Cubiss, A. Algora, M. Au, M. Balogh, S. Bara, R.A. Bark, C. Bernerd, M.J.G. Borge, D. Brugnara, K. Chrysalidis, T.E. Cocolios, H.D. Witte, Z. Favier, L.M. Fraile, H.O.U. Fynbo, A. Gottardo, R. Grzywacz, R. Heinke, A. Illana, P.M. Jones, D.S. Judson, A. Korgul, U. Köster, M. Labiche, L. Le, R. Lic, M. Madurga, N. Marginean, B.A. Marsh, C. Mihai, E. Nácher, C. Neacsu, C. Nita, B. Olaizola, J.N. Orce, C.A.A. Page, R.D. Page, J. Pakarinen, P. Papadakis, A. Perea, M.P.-S. kowska, Z. Podolyák, E. Reis, S. Rothe, M. Sedlak, C. Sotty, S. Stegemann, O. Tengblad, S.V. Tolokonnikov, J.M.U. ás, P.V. Duppen, N. Warr, W. Wojtaczka, Charge radii of thallium isotopes near the $N = 126$ shell closure, Phys. Rev. C 110 (2024) 34315. https://doi.org/10.1103/PhysRevC.110.034315